Carbohydrate Polymers 88 (2012) 1061–1071

Contents lists available at SciVerse ScienceDirect

Carbohydrate Polymers

journal homepage: www.elsevier.com/locate/carbpol

Structural changes during starch pasting using simultaneous Rapid Visco Analysis and small-angle neutron scattering

James Doutch[a], Mark Bason[b], Ferdi Franceschini[a], Kevin James[b], Douglas Clowes[a], Elliot P. Gilbert[a,*]

[a] Bragg Institute, Australian Nuclear Science and Technology Organisation, Locked Bag 2001, Kirrawee DC, NSW 2232, Australia
[b] Perten Instruments P/L, PO Box 70, North Ryde BC, NSW 1670, Australia

ARTICLE INFO

Article history:
Received 18 November 2011
Received in revised form 19 January 2012
Accepted 20 January 2012
Available online 28 January 2012

Keywords:
Starch
Rheology
Rapid Visco Analysis
Small-angle neutron scattering
Gelatinisation
Pasting

ABSTRACT

Rapid Visco Analysis (RVA) is an industry-wide method extensively used for determining the viscous properties of starch slurries enabling information to be extracted on pasting properties; however little is known about structural changes that occur during standard protocols. A commercial RVA instrument was modified to allow the passage of a neutron beam through its heating block and paddle assembly to enable the simultaneous measurement of SANS and RVA on a variety of commercial starches. SANS measurements were made at 1 min intervals throughout a standard 13 min RVA process across a q range of 0.018–0.2 Å^{-1}. In each of the starches, the well-known lamellar structure was observed up to the point at which the viscosity began to increase markedly. At this stage, the lamellar structure transformed instantaneously; the scattering patterns are indicative of the formation of a large scale structure with no apparent semi-crystalline properties and whose spatial arrangement may be analysed in terms of a fractal-like gel. The basic building blocks of this gel, under the assumption that they are spheroidal, appear to have dimensions of approximately 1 nm across all the starches tested. The sizes of the aggregates formed are several times larger and were found to vary across the time course of the experiment.

1. Introduction

Starch is the key carbohydrate in the human diet and the major storage polysaccharide in plants. It also finds increasing use in the polymer and pharmaceutical industries, in particular biofuels. The starch granule in the native state possesses a hierarchical structure from the micron- down to the nano-scale. This directly influences a number of properties of relevance from both a physiological and industrial perspective. Viscosity, and changes thereof during the pasting process (Atwell, Hood, Lineback, Varriano-Marston, & Zobel, 1988), is one such factor although the nano-scale structural changes that accompany such transitions are poorly understood.

Starch pasting rheology has commonly been studied with a Rapid Visco Analyser (Colombo, Leon, & Ribotta, 2011; Crosbie & Ross, 2007; Gomand, Lamberts, Visser, & Delcour, 2010; Wrigley, Booth, Bason, & Walker, 1996). In this device, the rotation of a pitched paddle impeller ensures that starch slurries are suspended during a controlled heating and cooling process. During a heating and cooling cycle in excess water, several changes in the RVA profile are observed. Firstly, a sufficient number of starch granules undergo rapid swelling and partial amylose leaching, particularly following gelatinisation, that a rapid rise in viscosity is observed. Under conditions of both heat and shear, the granules are partially disrupted and the leached amylose aligns leading to a reduction in viscosity in most cases. On subsequent cooling, the hydrated polymers re-associate and the material undergoes a transition to a gel type structure observed as a 'setback' or increase in viscosity (illustrated in Fig. 3(a)). The sum of these processes can be observed in the classic RVA pasting curve. The relationship between viscosity, as measured in an RVA, and average shear rates has been described by Lai, Steffe, and Ng (2000). Putseys, Gommes, Van Puyvelde, Delcour, and Goderis (2011) recently reported on the gelation behaviour of heat treated aqueous starch, with in situ rheometry in a Couette configuration using synchrotron SAXS. They determined that the scattering patterns obtained in this configuration suggested the formation of cylindrical scattering objects, growing into larger fractal aggregates upon cooling.

Starch is deposited in granules that show considerable botanical variation in shape and size distribution; generally granules range from 2 μm to 100 μm in dimension (Jane, Kasemsuwan, Leas, Zobel, & Robyt, 1994; Perez & Bertoft, 2010). Most of the dry weight of

* Corresponding author at: Bragg Institute, Australian Nuclear Science and Technology Organisation, Locked Bag 2001, Kirrawee DC, NSW 2232, Australia.
E-mail address: elliot.gilbert@ansto.gov.au (E.P. Gilbert).

0144-8617/$ – see front matter © 2012 Elsevier Ltd. All rights reserved.
doi:10.1016/j.carbpol.2012.01.066

the starch granule is composed of essentially linear amylose and highly branched amylopectin, the exact ratio varying considerably depending on genomic origin (Takeda, Hizukuri, Takeda, & Suzuki, 1987). The granules are further subdivided into growth ring structures, which are generally accepted to alternate between amorphous and semi-crystalline structures. This alternation is not well understood biophysically but in at least some plants may have its origin in variable diurnal deposition patterns. The semi-crystalline rings have been shown to consist of alternating 'crystalline' and 'amorphous' structures, with a repeating periodicity of approximately 90–100 Å which is readily observed using small angle neutron and X-ray scattering (SAXS/SANS) of hydrated granules (Blazek & Gilbert, 2011; Cameron & Donald, 1992; Waigh, Gidley, Komanshek, & Donald, 2000). At smaller length scales, wide angle X-ray scattering has demonstrated the existence at the molecular level of various crystal lattice types; for example, so-called A-type crystal structures being observed for cereal starches and B-type starches being observed for tubers and high amylose starches; these have monoclinic and hexagonal unit cells, respectively (Perez & Bertoft, 2010; Salman et al., 2009). There is now acceptance that there exists an intermediate level of organisation between the lamellae and growth rings. Indeed, the use of imaging techniques such as AFM on starch granules has provided some evidence for so-called blocklets; however very little is known about the details of these structures at present (see Perez & Bertoft, 2010 for review).

In general, when starch granules are heated in excess water above approximately 60 °C, the semi-crystalline structure of the starch granule is disrupted; although, in high amylose starches this occurs at higher temperature (Shi, Capitani, Trzasko, & Jeffcoat, 1998). A variety of granular, growth ring and molecular level mechanisms are thought to interplay in this process (Jenkins & Donald, 1998; Putseys et al., 2011; Vermeylen et al., 2006; Waigh et al., 2000) and the transition is irreversible. Specifically, the granules undergo a swelling process, accompanied by extensive changes in water distribution within the granule. There is also a loss of crystalline component and amylose leaching (Waigh et al., 2000). The gelatinisation behaviour of starch slurries has been studied previously using scattering techniques (I'Anson, Mile, Morris, Ring, & Nave, 1988; Jenkins & Donald, 1998; Putseys et al., 2011; Vallera, Cruz, Ring, & Boue, 1994). Cameron and Donald (1992) demonstrated that crystallinity was mainly lost during the endothermic phase of gelatinisation, after water appeared to enter the amorphous growth rings, with the crystalline regions appearing relatively unaffected during this early phase. They postulated that, beyond a critical level of swelling, stresses imposed on molecules in the semi-crystalline layers would eventually destroy the crystallinity. Vallera et al. (1994) performed SANS measurements across a wide q-range in amylose gels and concluded that the scattering spectra were not consistent with those that would be expected from true independent scattering particles such as spheres or rods; as a result, they analysed the gelation in terms of a biphasic polymer structure, with the polymer-rich phase organised into aggregated clusters that have a fractal structure. The fractal dimension of the final structures was found to be consistent with diffusion-limited aggregation.

Neutrons have several key advantages for analysing the nanostructure of food systems, in particular their relatively high penetration through dense or concentrated samples and sample environments as well as the ability to avoid beam damage relative to more intense synchrotron X-rays (Lopez-Rubio & Gilbert, 2009). We make use of these particular attributes to enable the simultaneous measurement of RVA and SANS, for the first time, to understand more fully the structural changes taking place during starch pasting.

2. Method

2.1. Small-angle neutron scattering

SANS experiments were conducted on the Quokka instrument at the Australian Nuclear Science and Technology Organisation (ANSTO) (Gilbert, Schulz, & Noakes, 2006). The instrument was operated at a wavelength, λ, of 5.078 Å with 14% wavelength resolution. All samples were prepared in D_2O at the same concentrations as typically used in RVA standard protocols as described below. Data were collected at equal source-to-sample (SSD) and sample-to-detector distance (SDD) of approximately 4 m with an aperture size = 7.5 mm yielding a q range of 0.018–0.200 $Å^{-1}$ where q is the magnitude of the scattering vector q defined as:

$$q = \frac{4\pi}{\lambda} \sin\,\theta \tag{1}$$

and 2θ is the scattering angle. One data set was also collected at longer distances of SSD ~ SDD ~ 20 m over a q range of 0.0039–0.0419 $Å^{-1}$ for tapioca starch, after completion of the RVA profile, to measure the structure of the material post-gelatinisation. Scattering from D_2O solvent sample in the RVA was collected and used as a scattering background. SANS datasets were reduced, normalised and radially averaged using a package of macros in Igor software originally written by Kline (2006) and modified to accept *HDF5* data files from Quokka. Scattering curves are plotted as absolute (SANS) intensity, I, versus q. SANS data collection was synchronised and initiated with a modification of the AACC standard 1 RVA H95 profile (AACC, 1999).

2.2. Rapid Visco Analyser

An RVA was modified to enable the simultaneous measurement of SANS. To do this a hole was drilled through the heating block to enable passage of the neutron beam. Additional borated aluminium shielding was installed to minimise activation of the RVA in addition to an upstream Cd aperture of 17.5 mm. Standard aluminium cans were used but the pitched paddle impeller was modified both to minimise scattering from the paddle itself and to ensure minimal multiple scattering (see Fig. 1). To do this, the plastic paddle, which would be a source of significant neutron scattering due to the large hydrogen content of the material, was replaced by one constructed from aluminium; the latter material has a significantly lower neutron scattering cross-section. Furthermore, a hollow, cylindrical band was incorporated into the centre of the paddle to ensure a scattering path length of 1 mm on either side between the outer surface of the paddle and the inner surface of the surrounding aluminium can. The performance of the paddle used was directly compared with the standard plastic paddle yielding highly comparable results. Samples were hydrated with D_2O instead of H_2O to significantly reduce the incoherent scattering background at a weight ratio of 3.00 g of starch–47.8 g of D_2O (equivalent to mass of 43.0 g of H_2O but taking into account the greater physical density of D_2O). Off-line comparison of H_2O and D_2O-hydrated starch shows that they are qualitatively similar (unpublished data).

A modified form of RVA Standard 1 (AACC, 1999) was used to provide a 13 min pasting profile, with maximum temperature of 95 °C. The temperature was held at a value of 25 °C for the first minute, and then allowed to ramp up to 95 °C, which was reached after an elapsed time of 4 min and 45 s. This temperature was then held until 7 min 15 s before being allowed to cool back down to 25 °C, after an elapsed time of 11 min; the device was held in this condition for a further 2 min. Samples were stirred at 960 rpm during the initial transmission measurement (2 min data collection). Thereafter, 1 min scattering runs were taken simultaneously with the RVA profile. Due to the mass of starch used in these experiments

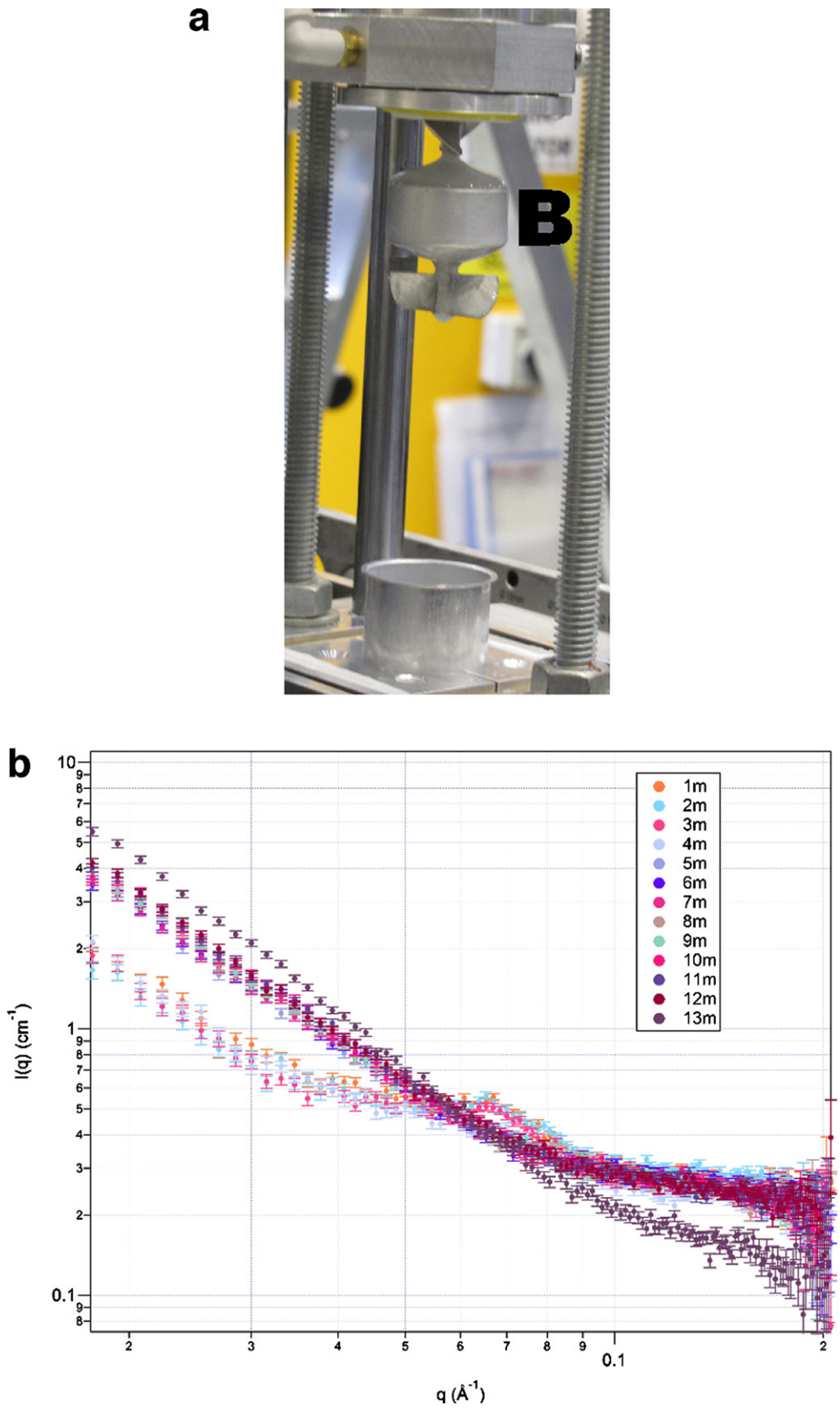

Fig. 1. (a) Modified paddle assembly for use in SANS/RVA experiments, hollow band through which neutrons pass is denoted by 'B'; (b) representative scattering patterns for waxy maize.

Table 1
Description and suppliers of starches used in this study. Compositional data from Swinkels (1985).

Starch	Vendor/description	Amylopectin content (%)	Amylose degree of polymerisation	Paste properties
Waxy maize	7350 Waxy number 1, Tate and Lyle, Decatur, IL	100	N/A	Long texture, fairly clear
Regular maize	PIAU Test Starch batch 770, Penford, NZ	72	800	Short texture, opaque
Wheat	Commercial material, Supermarket (Sydney, AU)	72	800	Short texture, cloudy
Regular potato starch	Commercial material, Supermarket (Sydney, AU)	79	3000	Long texture, very clear
Tapioca starch	Penford, Sydney, NSW, AU	83	3000	Long texture, very clear
Acid modified maize	Acid hydrolysed, low viscosity, ADM, Decatur, IL	Unavailable	Unavailable	Very short texture, opaque

it was necessary to increase the rotational speed of the paddle to 640 rpm after an initial 2 min stirring at 960 rpm. This was reduced to the standard 320 rpm after an elapsed time of 2 min 18 s i.e. the time at which the temperature has reached 50 °C. This was found to prevent settling of ungelatinised starch granules in the sample. The starches used in this study are summarised in Table 1.

3. Results

SANS data were found to be divided into two regimes for all the starches tested. The first was the well-known lamellar scattering (e.g. Cameron & Donald, 1992) and is analysed here using a combined Lorentzian peak and power law function (e.g. Blazek & Gilbert, 2010), given by Eq. (2) where A is the power law prefactor, δ is the power law decay, I_0 is the height of the peak, B is the half width at half maximum, and β is the background:

$$I(q) = Aq^{-\delta} + I_0\left[1 + \frac{(q-q_0)}{B^2}\right]^{-1} + \beta \quad (2)$$

With this method, the position and width in q-space of the peak and terminal power-law dependence are readily quantified. The second regime was found to manifest itself with the dramatic disappearance of lamellar scattering and a change in q-dependence during the RVA measurement. The q-dependence was found to take the form of non-integer values between −2 and −3, which is often indicative of mass fractal structures. Scattering patterns within this second regime were therefore analysed using a fractal model composed of polydisperse spheroidal building blocks, as described by Eq. (3) (Teixeira, 1988):

$$I(q) = \left[1 + \frac{\sin(D_f - 1)\tan^{-1}(q\xi)}{(qR_0)^{D_f}} \frac{D_f\Gamma(D_f-1)}{[1+1/(q^2\xi^2)]^{(D_f-1)/2}}\right] P(q) + \beta \quad (3)$$

where $I(q)$ is the scattering intensity, D_f is the fractal dimension, ξ is the correlation length, R_0 is the average radius of the building block particles and $P(q)$ is the form factor scattering from randomly distributed polydisperse spheres (Kotlarchyk & Chen, 1983). The data here are placed on an absolute scale; the scattering length density of deuterium oxide (6.36×10^{-6} Å^{-2}) and the scattering length density of the building block, assumed to be 3.8×10^{-6} Å^{-2} (Blazek & Gilbert, 2011) were fixed in this model. The volume fraction, block radius polydispersity, correlation length, ξ and fractal dimension D_f, were allowed to vary. The correlation length of the system is related to a generalised radius of gyration according to Eq. (4) (Teixeira, 1988):

$$R_g^2 = \frac{D_f(D_f+1)\xi^2}{2} \quad (4)$$

The effective radius of gyration shows interesting variations throughout the time course of the experiment in each starch investigated and provides a better indication of the aggregate size than the correlation length. In addition, R_g also appears to correlate with differences in viscosity between the starches studied (except acid modified maize) where larger values for R_g occur for systems exhibiting greater viscosity. Maize, acid modified maize and wheat show a general trend in which aggregate size may be correlated with increases and decreases in viscosity as detected by RVA.

RVA parameters are given in Table 2, showing the pasting temperatures and characteristic viscosities for each starch used in this study (annotated RVA profile shown in Fig. 3a). Waxy maize and tapioca achieve peak viscosity at relatively low temperature (<83 °C) compared with the normal maize (~95 °C). Potato exhibits the highest peak viscosity (442 cP) and has a comparatively small setback (6 cP). Waxy maize and tapioca have similarly large peak viscosity (221 and 265 cP, respectively). Wheat, normal maize and potato have relatively low setback, with tapioca having the greatest value (261 cP). The acid modified maize achieves a very low peak viscosity of 13 cP.

SANS fitting parameters are shown in Tables 3 and 4. While the scattering characterised by power law decay between −1 and −3 may be interpreted to originate from mass fractal structures (Teixeira, 1988), this simple scaling law is not applicable near $q < \xi^{-1}$ i.e. in the present case, in the limit of fractal gel behaviour. If this region is observable in the scattering data, this simple power-law relationship breaks down. It was found in the present study that D_f may be obtained directly from the power law behaviour in waxy maize, tapioca and potato. In the remainder of the samples, it was necessary to allow D_f to be freely fitted from Eq. (3). Typical representative 1D radially averaged scattering is shown for waxy maize in Fig. 2(a). False coloured representations of scattering as a function of time with viscosity transposed are shown in Fig. 3(a–f) with intensity represented on a logarithmic scale. They show the classic lamellar scattering (Blazek & Gilbert, 2011) being replaced, almost at the same time as the RVA viscosity increases, by a dramatic rise in scattering at low q values (corresponding to the formation of larger scale structures). This is seen to increase towards the end of the RVA profile.

Table 2
RVA parameters for all starches.

Starch	Pasting temperature (°C)	Peak viscosity (cP)	Final viscosity (cP)	Holding strength (cP)	Setback (cP)
Waxy maize	82.5	221	205	157	48
Maize	93.5	117	94	93	4
Wheat	93.5	91	74	71	6
Potato	78.4	442	399	422	6
Tapioca	80.3	265	410	183	261
Acid modified maize	95.0	13	18	11	7

Table 3
Power law plus Lorentzian fitting parameters for granular starch; lamellar spacing calculated from peak position (errors shown in brackets are one standard deviation).

Starch type	Time (min)	1	2	3	4
	Power law prefactor, A	0.0007 (0.0002)	0.0004 (0.0002)	0.0002 (0.001)	0.0003 (0.0001)
	(−)Power	1.94 (0.11)	2.07 (0.13)	2.26 (0.15)	2.17 (0.13)
	Scale factor, I0	0.16 (0.01)	0.18 (0.01)	0.20 (0.01)	0.13 (0.01)
Waxy maize	Peak position ($Å^{-1}$)	0.065 (0.001)	0.065 (0.001)	0.063 (0.001)	0.063 (0.001)
	Peak hwhm ($Å^{-1}$)	0.012 (0.001)	0.013 (0.001)	0.016 (0.001)	0.016 (0.002)
	Bgd (cm^{-1})	0.232 (0.006)	0.254 (0.004)	0.223 (0.003)	0.207 (0.004)
	Lamellar spacing (Å)	96.7 (1.5)	96.7 (1.5)	99.7 (1.6)	99.7 (1.6)
	Power law prefactor, A	0.0002 (0.0001)	0.0002 (0.0001)	0.0002 (0.0001)	0.0003 (0.0001)
	(−)Power	2.22 (0.19)	2.19 (0.17)	2.27 (0.19)	2.08 (0.12)
	Scale factor, I0	0.10 (0.01)	0.09 (0.01)	0.07 (0.01)	0.06 (0.01)
Maize	Peak position ($Å^{-1}$)	0.063 (0.002)	0.064 (0.001)	0.064 (0.003)	0.064 (0.002)
	Peak hwhm ($Å^{-1}$)	0.019 (0.003)	0.016 (0.003)	0.021 (0.004)	0.013 (0.003)
	Bgd (cm^{-1})	0.253 (0.004)	0.273 (0.003)	0.235 (0.004)	0.214 (0.004)
	Lamellar spacing (Å)	99.7 (3.2)	98.2 (1.5)	98.2 (4.6)	98.2 (3.1)
	Power law prefactor, A	0.0002 (0.0001)	9E−05 (6E−05)	0.0002 (0.0001)	0.0006 (0.0002)
	(−)Power	2.16 (0.20)	2.33 (0.17)	2.20 (0.17)	1.96 (0.10)
	Scale factor, I0	0.10 (0.01)	0.10 (0.01)	0.10 (0.01)	0.05 (0.01)
Wheat	Peak position ($Å^{-1}$)	0.065 (0.002)	0.064 (0.001)	0.064 (0.001)	0.065 (0.002)
	Peak hwhm ($Å^{-1}$)	0.018 (0.003)	0.016 (0.002)	0.017 (0.003)	0.011 (0.004)
	Bgd (cm^{-1})	0.233 (0.004)	0.256 (0.003)	0.211 (0.003)	0.189 (0.005)
	Lamellar spacing (Å)	96.7 (3.0)	98.2 (1.5)	98.2 (1.5)	96.7 (3.0)
	Power law prefactor, A	3.92E−05 (1.49E−05)	5.28E−05 (3.47E−05)	5.45E−05 (2.33E−05)	0.00014 (0.00004)
	(−)Power	2.55 (0.10)	2.39 (0.18)	2.46 (0.12)	2.30 (0.08)
	Scale factor, I0	0.020 (0.01)	0.020 (0.007)	0.024 (0.007)	0.026 (0.01)
Potato	Peak position ($Å^{-1}$)	0.070 (0.002)	0.066 (0.003)	0.066 (0.002)	0.061 (0.002)
	Peak hwhm ($Å^{-1}$)	0.005 (0.003)	0.008 (0.005)	0.008 (0.004)	0.003 (0.003)
	Bgd (cm^{-1})	0.199 (0.002)	0.213 (0.002)	0.180 (0.002)	0.169 (0.003)
	Lamellar spacing (Å)	89.8 (2.6)	95.2 (4.3)	95.2 (2.9)	103.0 (3.4)
	Power law prefactor, A	0.0002 (0.0001)	0.0002 (0.0001)	9.33E−05 (6.32E−05)	0.0002 (0.0001)
	(−)Power	2.14 (0.15)	2.19 (0.22)	2.35 (0.18)	2.20 (0.12)
	Scale factor, I0	0.12 (0.01)	0.13 (0.01)	0.13 (0.01)	0.07 (0.01)
Tapioca	Peak position ($Å^{-1}$)	0.065 (0.001)	0.064 (0.001)	0.062 (0.001)	0.064 (0.001)
	Peak hwhm ($Å^{-1}$)	0.012 (0.002)	0.014 (0.002)	0.016 (0.002)	0.013 (0.003)
	Bgd (cm^{-1})	0.226 (0.003)	0.242 (0.004)	0.198 (0.002)	0.192 (0.003)
	Lamellar spacing (Å)	96.7 (1.5)	98.2 (1.5)	101.3 (1.6)	98.2 (1.5)
	Power law prefactor, A	0.0005 (0.0001)	0.0010 (0.0003)	0.0009 (0.0002)	0.0012 (0.0003)
	(−)Power	2.22 (0.08)	2.00 (0.07)	2.02 (0.07)	1.95 (0.07)
	Scale factor, I0	0.320 (0.013)	0.26 (0.01)	0.24 (0.01)	0.149 (0.012)
Acid modified maize	Peak position ($Å^{-1}$)	0.064 (0.001)	0.064 (0.001)	0.064 (0.001)	0.064 (0.001)
	Peak hwhm ($Å^{-1}$)	0.016 (0.001)	0.015 (0.001)	0.013 (0.001)	0.013 (0.002)
	Bgd (cm^{-1})	0.379 (0.004)	0.382 (0.006)	0.362 (0.005)	0.340 (0.006)
	Lamellar spacing (Å)	98.2 (1.5)	98.2 (1.5)	98.2 (1.5)	98.2 (1.5)

For the tapioca gel structure, a final measurement was taken in the low q region. This was achieved by adjusting the collimation and detector distances to the maximum 20 m. This measurement was taken in a 30 min data set at the end of the RVA pasting procedure, and for the purposes of fitting, was combined with the higher-q data from the scan analysed in Table 5. The combined scattering pattern is shown in Fig. 4. These data were fitted using the fractal algorithm used previously and the results are shown in Table 4. The fractal fit was performed with a minimum q value of 0.007 $Å^{-1}$; at smaller values, the q-dependence of the scattering changes markedly. The unified model (Beaucage, 1996) was used to fit a function with power law −3.97 and prefactor 9.97×10^{-8}. The unified model is given by Eq. (5):

$$I(q) = G\exp\left(-\frac{q^2R_g^2}{3}\right) + B\left\{\frac{[erf(qR_g/6^{0.5})]^3}{q}\right\}^P \quad (5)$$

where G and B are the Guinier and Power law prefactors, respectively, R_g is the generalised particle radius of gyration and P the power law decay. This equation can be used to fit simple power laws under the assumption that $G = 0$ and R_g is arbitrarily large. This equation may be applied to obtain fitting parameters for the very small low q tail region in the tapioca scans at the limit of fractal behaviour.

4. Discussion

The first simultaneous SANS/RVA experiment has been performed to analyse the structural changes that take place during starch pasting. From an initial principal lamellar structure, the starches under investigation consistently form extended networks across the time course of the experiment. As expected, the starches display variations in their pasting behaviour as demonstrated in the RVA curves. The potato and waxy maize reached much higher peak viscosity, with the other maize starches and wheat being lower. Waxy maize and tapioca both exhibit considerable setback. The final viscosities from the starches studied fall into essentially two groups, with waxy maize, tapioca and potato being much more viscous than maize or wheat, in line with previous investigations (Swinkels, 1985).

Up to the point at which the viscosity starts to increase, the SANS data exhibit the well-known lamellar structure of starch which does not appear to undergo any significant change in any of the varieties tested, within the time binning resolution of this experiment. There is however some variance in the power-law dependence of the scattering curve but which is close to a value of −2 consistent with a lamellar structure up to the point of the viscosity increase. We note that this region of the scattering curve will be affected by substructures larger than the lamellae, most notably growth rings, blocklets or clusters, with some degree of surface scattering from the granules themselves albeit with their

Table 4
Fractal fitting parameters for starch pastes.

Starch type	Time (min)	5	6	7	8	9	10	11	12	13
	Volume fraction	0.021 (0.001)	0.021 (0.001)	0.023 (0.001)	0.021 (0.001)	0.023 (0.001)	0.019 (0.001)	0.023 (0.001)	0.024 (0.001)	0.032 (0.001)
	Block radius (Å)	5.0	5.0	5.0	5.0	5.0	5.0	5.0	5.0	5.0
	Block polydispersity	0.1	0.1	0.1	0.1	0.1	0.1	0.1	0.1	0.1
Waxy maize	Fractal dimension	2.28[a] (0.03)	2.29[a] (0.02)	2.24[a] (0.03)	2.32[a] (0.03)	2.27[a] (0.03)	2.40[a] (0.03)	2.31[a] (0.03)	2.28[a] (0.02)	2.31[a] (0.02)
	Correlation length (Å)	120.9 (19.3)	108.1 (12.5)	124.3 (18.3)	101.7 (11.4)	121.3 (18.3)	92.3 (10.5)	112.2 (12.7)	138.3 (24.2)	108.7 (9.7)
	bkgd (cm^{-1})	0.211 (0.002)	0.218 (0.002)	0.208 (0.002)	0.213 (0.002)	0.208 (0.002)	0.214 (0.002)	0.204 (0.002)	0.199 (0.002)	0.095 (0.002)
	Guinier Rad cluster (Å)	233.8	209.8	236.8	199.6	233.7	186.5	219.4	267.5	212.4
	Volume fraction	0.009 (0.001)	0.011 (0.001)	0.012 (0.001)	0.010 (0.001)	0.010 (0.001)	0.011 (0.001)	0.012 (0.001)	0.014 (0.001)	0.022 (0.001)
	Block radius (Å)	5.0	5.0	5.0	5.0	5.0	5.0	5.0	5.0	5.0
	Block polydispersity	0.1	0.1	0.1	0.1	0.1	0.1	0.1	0.1	0.1
Maize	Fractal dimension	2.82 (1.9)	2.80 (0.07)	2.68 (0.07)	2.81 (0.06)	2.88 (0.05)	2.88 (0.05)	2.85 (0.05)	2.78 (0.05)	2.71 (0.03)
	correlation length (Å)	31.873 (2.0)	35.2 (2.6)	40.9 (3.3)	36.9 (2.5)	36.7 (2.0)	37.8 (2.1)	39.0 (2.0)	42.3 (2.5)	45.4 (2.4)
	bkgd (cm^{-1})	0.228 (0.004)	0.229 (0.003)	0.226 (0.004)	0.232 (0.003)	0.231 (0.003)	0.230 (0.003)	0.223 (0.003)	0.217 (0.003)	0.114 (0.003)
	Guinier rad cluster Å	74.0	81.2	90.8	85.4	86.8	89.4	91.3	97.2	101.7
	Volume fraction	0.011 (0.001)	0.010 (0.001)	0.011 (0.001)	0.013 (0.001)	0.011 (0.001)	0.012 (0.001)	0.015 (0.001)	0.014 (0.001)	0.019 (0.001)
	Block radius (Å)	5.0	5.0	5.0	5.0	5.0	5.0	5.0	5.0	5.0
	Block polydispersity	0.1	0.1	0.1	0.1	0.1	0.1	0.1	0.1	0.1
Wheat	Fractal dimension	2.78 (0.08)	2.81 (0.06)	2.73 (0.07)	2.69 (0.06)	2.86 (0.05)	2.90 (0.05)	2.76 (0.05)	2.78 (0.04)	2.79 (0.04)
	Correlation length (Å)	33.9 (2.4)	37.6 (2.4)	41.8 (3.3)	43.1 (3.0)	37.1 (1.9)	36.6 (2.1)	42.2 (2.4)	42.7 (2.4)	40.2 (1.7)
	bkgd (cm^{-1})	0.211 (0.004)	0.216 (0.003)	0.216 (0.003)	0.212 (0.003)	0.209 (0.003)	0.206 (0.003)	0.201 (0.003)	0.205 (0.003)	0.103 (0.003)
	Guinier rad cluster (Å)	77.9	87.0	94.3	96.2	87.2	87.0	96.2	97.8	92.5
	Volume Fraction	0.030 (0.001)	0.039 (0.001)	0.0382 (0.001)	0.0323 (0.001)	0.0280 (0.001)	0.0329 (0.001)	0.0331 (0.001)	0.0338 (0.001)	0.032 (0.001)
	Block Radius (Å)	5.0	5.0	5.0	5.0	5.0	5.0	5.0	5.0	5.0
	block polydispersity	0.1	0.1	0.1	0.1	0.1	0.1	0.1	0.1	0.1
Potato	fractal dimension	2.11	2.15	2.15	2.12	2.18	2.19	2.21	2.21	2.26
	correlation length (Å)	194.2 (61.0)	137.1 (15.8)	149.2 (25.5)	186.1 (51.8)	184.4 (60.4)	143.5 (19.9)	152.099 (28.8)	146.2 (27.1)	132.3 (23.6)
	bkgd (cm^{-1})	0.073 (0.002)	−0.006 (0.001)	−0.001 (0.001)	0.066 (0.002)	0.072 (0.002)	0.014 (0.002)	−0.002 (0.001)	−0.006 (0.002)	−0.002 (0.001)
	Guinier rad cluster (Å)	351.7	252.2	274.6	338.3	343.2	268.1	286.5	275.3	253.8
	Volume Fraction	0.028 (0.001)	0.021 (0.001)	0.022 (0.001)	0.025 (0.001)	0.028 (0.001)	0.026 (0.001)	0.032 (0.001)	0.042 (0.001)	0.042 (0.001)
	Block Radius (Å)	5.0	5.0	5.0	5.0	5.0	5.0	5.0	5.0	5.0
	block polydispersity	0.1	0.1	0.1	0.1	0.1	0.1	0.1	0.1	0.1
Tapioca	fractal dimension	2.04[a] (0.03)	2.19[a] (0.03)	2.12[a] (0.04)	2.15[a] (0.03)	2.10[a] (0.03)	2.14[a] (0.03)	2.19[a] (0.02)	2.21[a] (0.02)	2.26[a] (0.02)
	correlation length (Å)	193.9 (70.0)	120.8 (21.0)	186.0 (74.0)	145.1 (30.0)	156.7 (40.0)	164.5 (50.0)	135.4 (21.3)	137.2 (17.3)	125.1 (15.9)
	bkgd (cm^{-1})	0.172 (0.002)	0.174 (0.002)	0.160 (0.002)	0.180 (0.002)	0.174 (0.002)	0.173 (0.002)	0.098 (0.002)	−0.013 (0.001)	−0.019 (0.001)
	Guinier Rad cluster (Å)	341.4	225.7	338.3	267.1	282.7	301.6	253.1	258.5	240.1
	Volume Fraction	0.014 (0.001)	0.0132 (0.001)	0.0128 (0.001)	0.008 (0.001)	0.008 (0.001)	0.009 (0.001)	0.010 (0.001)	0.013 (0.001)	0.019 (0.001)
	Block Radius (Å)	5	5	5	5	5	5	5	5	5
	block polydispersity	0.1	0.1	0.1	0.1	0.1	0.1	0.1	0.1	0.1
Acid modified maize	fractal dimension	2.65 (0.05)	2.68 (0.05)	2.59 (0.05)	2.89 (0.06)	2.93 (0.05)	2.92 (0.05)	2.95 (0.05)	2.80 (0.04)	2.78 (0.03)
	correlation length (Å)	44.0 (3.1)	47.7 (4.0)	58.9 (5.0)	40.8 (3.0)	39.9 (2.3)	41.1 (2.3)	39.3 (2.2)	45.3 (2.4)	46.9 (2.2)
	bkgd (cm^{-1})	0.223 (0.003)	0.232 (0.003)	0.259 (0.003)	0.285 (0.003)	0.282 (0.003)	0.280 (0.003)	0.280 (0.003)	0.267 (0.003)	0.172 (0.003)
	Guinier Rad	96.6	106.0	126.7	96.5	95.8	98.3	94.7	104.6	107.3

[a] Denotes value obtained through power law fitting (errors shown in brackets are one standard deviation)

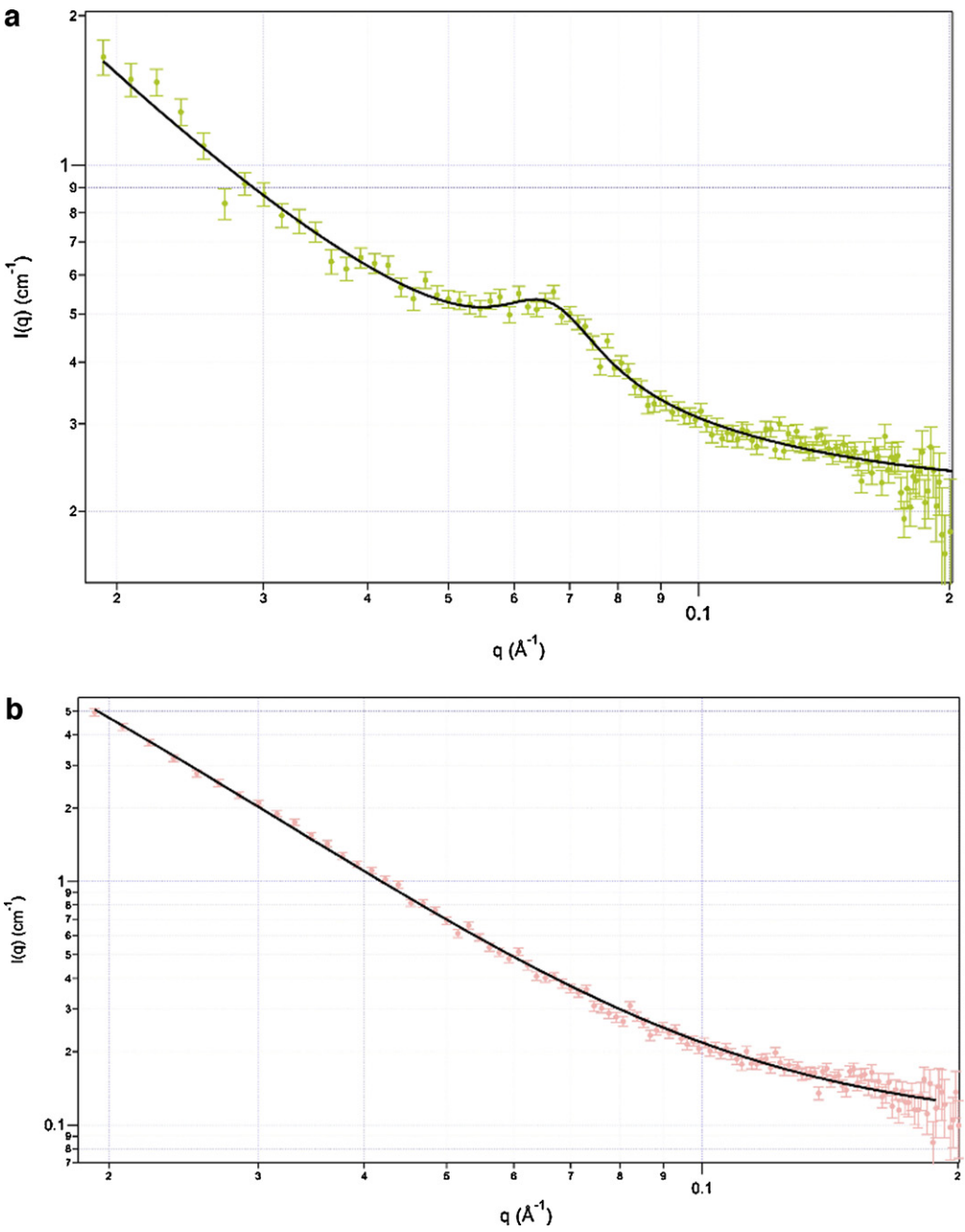

Fig. 2. (a) Representative power-law fit and (b) fractal fit (fit lines in bold) to SANS for waxy maize starch after 2 min and 6 min.

origin at lower q. Changes in this region may be related to some form of swelling occurring within the granule. The maintenance of the lamellar peak and $q^{\sim -2}$ behaviour are consistent with previous studies and indicates that, prior to and including the sudden viscosity increase, swelling primarily affects the amorphous growth rings (Jenkins & Donald, 1998), with little change in the semicrystalline rings.

After the viscosity has reached a peak, the lamellar scattering is no longer present; the scattering pattern can now be described with a power law between −2 and −3. This implies a mass fractal regime (Beaucage, 1996; Teixeira, 1988) indicating the formation of a networked, branched polymer structure across these length scales. These aggregated structures seem to have sizes that cover the detectable range probed in these experiments. It is instructive to compare these fractal dimensions with other systems such as linear swollen polymers ($D_f = 5/3$), polymer in a theta solvent ($D_f = 2$), randomly branched Gaussian chains ($D_f = 16/7$) and diffusion limited aggregates (2.5) (Beaucage, 1996). Malcai et al. (1997) give a detailed list of fractal dimensions for a wide variety of systems.

In their SAXS measurements, Putseys et al. (2011) used a fixed fractal dimension of 2.6 to fit their data; under this constraint the size of the fractal networks was rather small in comparison with the building block particle. Our data suggest that an improved approach is to obtain the fractal dimension (D_f) value from either power law fitting or actually allowing it to refine during fitting; the appropriate method can be determined by inspection of the scattering curves (Teixeira, 1988).

The fractal scattering model suggests that the building block particles of the gels are close to 1 nm; however this is somewhat difficult to verify in this system due to the presence of finite incoherent background scattering, primarily associated with hydrogen atoms in the starch. Inspection of the scattering curve suggests that

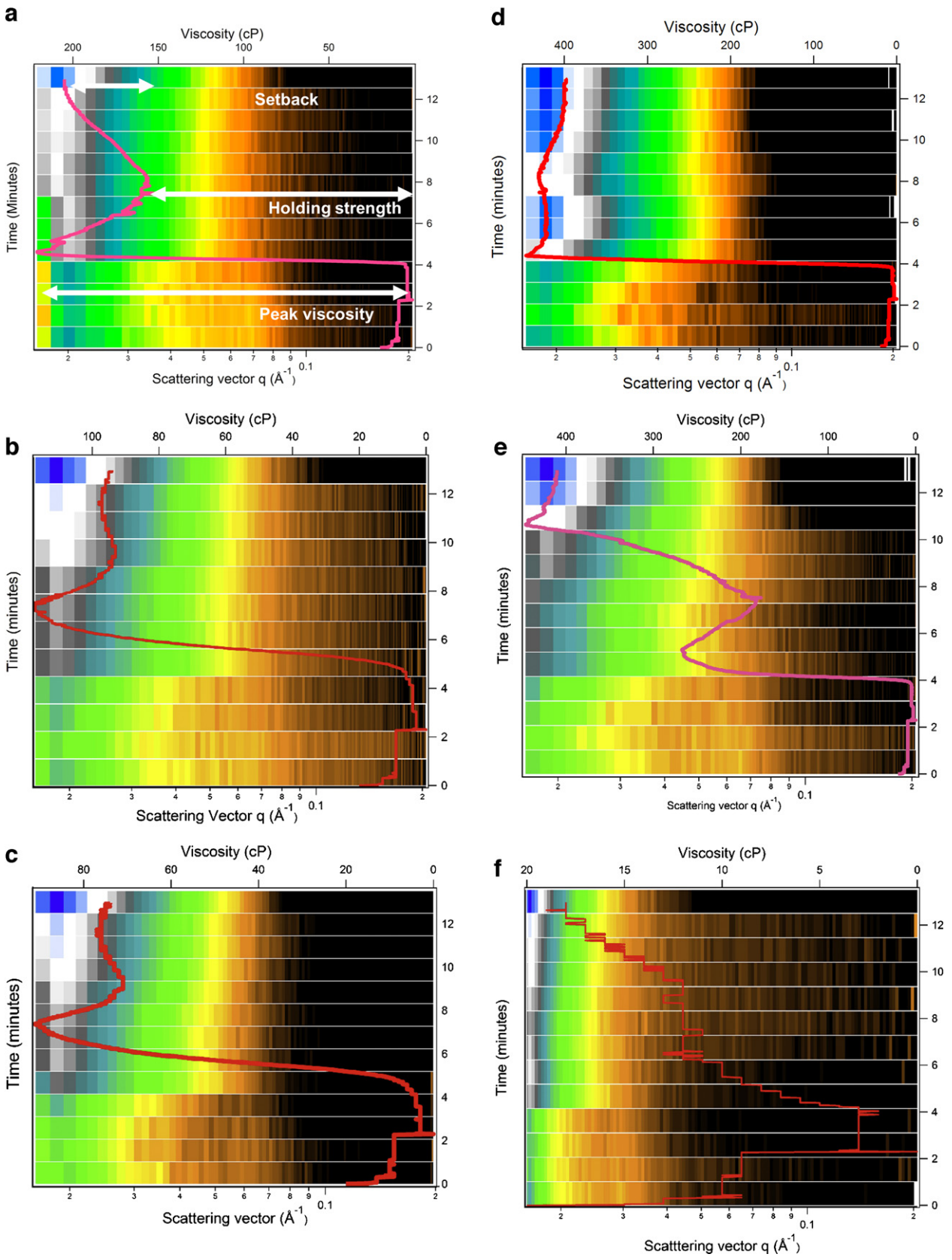

Fig. 3. Combined SANS data with RVA profiles for: (a) waxy maize (RVA profile annotated), (b) maize, (c) wheat, (d) potato, (e) tapioca and (f) highly acid modified maize. Black and white regions represent low and high intensity, respectively (logarithmic scale).

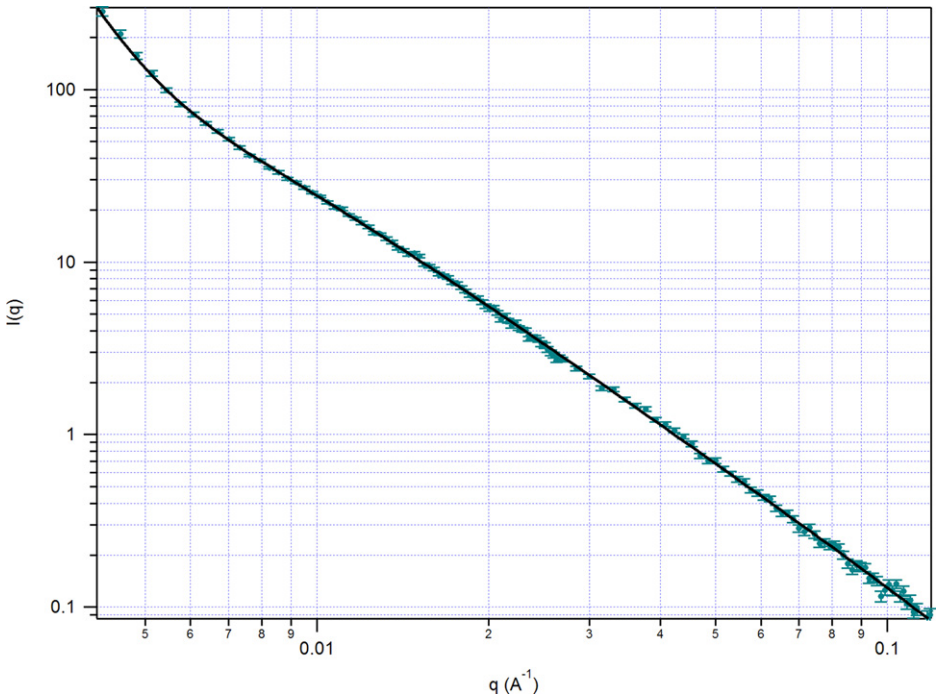

Fig. 4. SANS data over extended q range at the conclusion of the tapioca RVA profile with corresponding fit using combined unified and fractal models.

this probably represents an upper value. The variation in background during the evolution of the RVA profile is likely to be caused by cumulative exchange of hydrogen (in the starch) for deuterium (in the solvent) during the processing of the material. A constant D_2O background is used for each sample thus, as further exchange occurs, the incoherent scattering background from the sample decreases and an increase in signal to noise is apparent at high scattering angle.

The fractal model, combined with the ability to collect intensity data on an absolute scale, suggests the scattering material occupies a plausible volume fraction of the sample, using the scattering length densities of D_2O and starch. Assuming physical densities of 1.11 g cm^{-3} and 1.55 g cm^{-3}, respectively, (Blazek & Gilbert, 2011) the volume fraction is calculated at 4.4%; this is in good agreement with our fitting parameters, in contrast to other potential models tested such as cylindrical objects. In the latter case, the observed volume fraction was found to be almost an order of magnitude lower than the expected value. There is a general trend in the fractal structures for the calculated volume fraction to increase during the time course of the experiment, suggesting that a fraction of the initial material has not been converted to a gelated system. This provides an excellent demonstration of the value of placing experimental SANS/SAXS data on an absolute scale.

Absolute intensity data have also allowed us to exclude other possible particle shapes and sizes for the gel structures; in particular we were unable to fit the data with models consisting of dilute cylindrical particles (Putseys et al., 2011) while ensuring physically plausible values for volume fraction. The latter 'blurry rod' model consists of a basic rod form factor convolved by an exponential function which acts to modulate the power law decay of the scattering patterns at high q values. This in effect means any power-law decay may be modelled by adding blurring or a very high degree of polydispersity to a basic shape such as a rod or sphere. In contrast, the fractal model has the advantage of being based on well-defined objects which highlights interesting differences both dynamically during RVA and between genomes, while maintaining a physically meaningful volume fraction.

Table 5
Fractal fitting parameters for combined mid and low q scan on Tapioca starch (errors are one standard deviation).

Volume fraction	0.042 (0.001)
Block radius (Å)	5.0
block polydispersity	0.10
Fractal dimension	2.234 (0.007)
Correlation length (Å)	291.1 (12.9)
bkgd (cm^{-1})	−0.020 (0.002)
Guinier rad cluster (Å)	553.1

Electron microscopy has demonstrated that amylopectin and amylose gels can form structures which have an almost cylindrical appearance at the micron length-scale (Putaux, Buleon, & Chanzy, 2000); however, these structures are highly distorted, almost worm-like, and exhibit branched and looped regions composed of networked, segmented chains that resemble a fractal structure. In amylopectin gels, the lateral width of each segment of the chain is approximately 100–150 Å with length 300–700 Å. These values are very similar to the effective R_g of the clusters reported in this work. It seems plausible therefore that the fractal fits presented in this paper represent the scattering from each segment or branch (a possible representation is given in Fig. 4, Beaucage, 1996) of the larger scale chains detected by other methods (Fannon & Bemiller, 1992; Putaux et al., 2000; Vallera et al., 1994). The application of USANS techniques to study the larger-scale structure of these systems would be valuable with analysis via the unified model (Beaucage, 1996) or a worm like model (Kholodenko, 1993). Furthermore, during the time resolution of this experiment, the transformation from a lamellar structure with semicrystalline growth rings into a gel network is rather abrupt. This transition region begs further study.

The scattering pattern from tapioca performed at the conclusion of the standard RVA measurement at the lowest q values is instructive in showing the different scattering regimes present in the starch pastes. A mass fractal regime with change of slope at 0.007 Å^{-1} is observed. There is then a transition into interfacial (−4) scattering down to the lowest q values measured. This possibly represents surface scattering from aggregated regions and the remnants ('ghosts') of starch granules (Fannon & Bemiller, 1992).

Previous SANS measurements on amylose gels have also demonstrated the presence of large-scale fractal networks (Vallera et al., 1994) extending up to several microns in size which may correlate to the large-scale fractal aggregates seen in amylose and amylopectin gels with electron microscopy (e.g. Putaux et al., 2000). In the case of the RVA, the shear forces will presumably limit the size of networks on the micron scale during the time course of the experiment.

In terms of fractal dimension, the samples appear to fall into two groups: those in which D_f is closer to 2 and those in which D_f falls closer to, but does not exceed, 3. It is of interest that waxy and normal maize fall into different groups. In waxy maize, tapioca and potato pastes, the network structures detected by SANS are relatively large, and indeed the values derived in this work are lower bounds, as demonstrated even within the extended q-range study on tapioca paste. It has been previously demonstrated that potato, waxy maize and tapioca-derived pastes have similar large-scale structure characteristics including texture (e.g. Swinkels, 1985) and our data would indicate that this is the origin of the observed low-q behaviour. The acid modified maize, conventional maize and wheat pastes have smaller aggregate sizes and the fractal dimensions are much higher than the other group. The fractal dimension of waxy maize appear to be intermediate to the potato/tapioca and wheat/maize groupings.

Relatively lower fractal dimensions in tapioca and potato pastes may indicate a less-branched or less complex structure (Beaucage, 2004) across the length scales probed in this work. Indeed, basic fitting of experimental data with Eq. (5) reinforces the idea that the objects in this study are not simple geometries such as rods, for example, by inspection of the connectivity dimension (c in Beaucage's notation) from the prefactors G and B (Beaucage, 2004). It can also be observed that the waxy maize pastes (containing solely highly branched amylopectin) seem to possess large aggregates of similar size to tapioca and potato pastes, but generally higher fractal dimension throughout the time course of the RVA measurement. The high D_f of wheat and maize starches may then correlate to a more complex structure and could indicate a high degree of polydispersity in the sizes of the fractal aggregates (Beaucage, 2004). In these cases the D_f may be perturbed slightly by scattering from granule ghosts (Fannon & Bemiller, 1992). The latter may limit the sizes of the fractal networks in this case.

The D_f and aggregate/network sizes show some variance during the time course of RVA. This hints at varying levels of disruption and re-association during a pasting curve. Generally, there appear to be interesting variations around the time at which the holding strength is reached, with the D_f values generally reaching a maximum around this point.

5. Conclusions

The nanometre-scale structural changes accompanying starch pasting have been measured for the first time using simultaneous SANS/RVA. There are found to be two scattering regimes present for all the starches examined in this study. The first regime consists of the well-described periodic lamellar peak and low q power-law behaviour; this type of scattering occurs approximately to the point at which peak viscosity occurs. The results appear to indicate that changes up to this point occur predominantly in the amorphous growth rings, in line with previous studies of starch gelatinisation. After this point, the lamellar structure disappears and the scattering takes the form of a mass-fractal structure. There appear to be interesting variations in the relative complexities of the structures formed and in the size of the fractal aggregates. Waxy maize, tapioca and potato appear to form relatively large aggregates. The RVA measurements indicate that these starches have the greatest viscosity. Starches exhibiting lower viscosity, namely normal and acid modified maize and wheat, have smaller network sizes. It is likely that the networks measured in this work can themselves aggregate into larger structures such as the worm-like structures seen with electron microscopy during retrogradation. The transition between lamellar and mass-fractal scattering is rather abrupt and provides an area for further study.

Acknowledgement

We would like to acknowledge Industry & Investment New South Wales who contributed a grant through its TechVouchers Program to partially support this work.

References

AACC. (1999). *General pasting method for wheat or rye flour using Rapid Visco Analyser, AACC Method 76-21, Approved Methods of Analysis* (9th ed.). St Paul, MN: American Association of Cereal Chemists.

Atwell, W. A., Hood, L. F., Lineback, D. R., Varriano-Marston, E., & Zobel, H. F. (1988). The terminology and methodology associated with basic starch phenomena. *Cereal Foods World*, *33*, 308–331.

Beaucage, G. (1996). Small-angle scattering from polymeric mass fractals of arbitrary mass-fractal dimension. *Journal of Applied Crystallography*, *29*, 134–146.

Beaucage, G. (2004). Determination of branch fraction and minimum dimension of mass-fractal aggregates. *Physical Review E*, *70*, 031401.

Blazek, J., & Gilbert, E. P. (2010). Effect of enzymatic hydrolysis on native starch granule structure. *Biomacromolecules*, *11*, 3275–3289.

Blazek, J., & Gilbert, E. P. (2011). Application of small-angle X-ray and neutron scattering techniques to the characterisation of starch structure: A review. *Carbohydrate Polymers*, *85*, 281–293.

Cameron, R. E., & Donald, A. M. (1992). A small-angle X-ray scattering study of the annealing and gelatinization of starch. *Polymer*, *33*, 2628–2636.

Colombo, A., Leon, A. E., & Ribotta, P. D. (2011). Rheological and calorimetric properties of corn-, wheat-, and cassava-starches and soybean protein concentrate composites. *Starch–Starke*, *63*, 83–95.

Crosbie, G. B., & Ross, A. S. (2007). *The RVA handbook*. St. Paul, MN: AACC.

Fannon, J. E., & Bemiller, J. N. (1992). Structure of corn starch paste and granule remnants revealed by low-temperature scanning electron microscopy after cryopreparation. *Cereal Chemistry*, *69*, 456–460.

Gilbert, E. P., Schulz, J. C., & Noakes, T. J. (2006). 'Quokka' – The small-angle neutron scattering instrument at OPAL. *Physica B: Condensed Matter*, *385–386*, 1180–1182.

Gomand, S. V., Lamberts, L., Visser, R. G. F., & Delcour, J. A. (2010). Physicochemical properties of potato and cassava starches and their mutants in relation to their structural properties. *Food Hydrocolloids*, *24*, 424–433.

I'Anson, K. J., Mile, M. J., Morris, V. J., Ring, S. G., & Nave, C. (1988). A study of amylose gelation using a synchrotron X-ray source. *Carbohydrate Polymers*, *8*, 45–53.

Jane, J.-L., Kasemsuwan, T., Leas, S., Zobel, H., & Robyt, J. F. (1994). Anthology of starch granule morphology by scanning electron microscopy. *Starch*, *46*, 121–129.

Jenkins, P. J., & Donald, A. M. (1998). Gelatinisation of starch: A combined SAXS/WAXS/SANS study. *Carbohydrate Research*, *308*, 133–147.

Kholodenko, A. L. (1993). Analytical calculation of the scattering function for polymers of arbitrary flexibility using the dirac propagator. *Macromolecules*, *26*, 4179–4183.

Kline, S. R. (2006). Reduction and analysis of SANS and USANS data using IGOR Pro. *Journal of Applied Crystallography*, *39*, 895–900.

Kotlarchyk, M., & Chen, S.-H. (1983). Analysis of small-angle neutron scattering spectra from polydisperse interacting colloids. *Journal of Chemical Physics*, *79*, 2461–2469.

Lai, K. P., Steffe, J. F., & Ng, P. K. W. (2000). Average shear rates in the Rapid Visco Analyser (RVA) mixing system. *Cereal Chemistry*, *77*, 714–716.

Lopez-Rubio, A., & Gilbert, E. P. (2009). Neutron scattering: A natural tool for food science and technology research. *Trends in Food Science and Technology*, *20*, 576–586.

Malcai, O., Lidar, D. A., & Biham, O. (1997). Scaling range and cutoffs in empirical fractals. *Physical Review E*, *56*, 2817–2827.

Perez, S., & Bertoft, E. (2010). The molecular structures of starch components and their contribution to the architecture of starch granules: A comprehensive review. *Starch/Starke*, *62*, 389–420.

Putaux, J.-L., Buleon, A., & Chanzy, H. (2000). Network formation in dilute amylose and amylopectin studied by TEM. *Macromolecules*, *33*, 6416–6422.

Putseys, J. A., Gommes, C. J., Van Puyvelde, P., Delcour, J. A., & Goderis, B. (2011). In situ SAXS under shear unveils the gelation of aqueous starch suspensions and the impact of added amylose–lipid complexes. *Carbohydrate Polymers*, *84*, 1141–1150.

Salman, H., Blazek, J., Lopez-Rubio, A., Gilbert, E. P., Hanley, T., & Copeland, L. (2009). Structure–function relationships in A and B granules from wheat starches of similar amylose content. *Carbohydrate Polymers*, *75*, 420–427.

Shi, Y-C., Capitani, T., Trzasko, P., & Jeffcoat, R. (1998). Molecular structure of a low-amylopectin starch and other high-amylose maize starches. *Journal of Cereal Science*, *27*, 289–299.

Swinkels, J. J. M. (1985). Composition and properties of commercial native starches. *Starch/Starke*, *37*, 1–5.
Takeda, Y., Hizukuri, S., Takeda, C., & Suzuki, A. (1987). Structures of branched molecules of amyloses of various origins, and molecular fractions of branched and unbranched molecules. *Carbohydrate Research*, *227*, 113–120.
Teixeira, J. (1988). Small-angle scattering by fractal systems. *Journal of Applied Crystallography*, *21*, 781–785.
Vallera, A. M., Cruz, M. M., Ring, S. G., & Boue, F. (1994). The structure of amylose gels. *Journal of Physics: Condensed Matter*, *6*, 311–320.
Vermeylen, R., Derycke, C., Delcour, J. A., Goderis, B., Reynaers, H., & Koch, M. H. J. (2006). Gelatinization of starch in excess water: Beyond the melting of lamellar crystallites: A combined wide- and small-angle X-ray scattering study. *Biomacromolecules*, *7*, 2624–2630.
Waigh, T. A., Gidley, M. J., Komanshek, B. U., & Donald, A. M. (2000). The phase transformations in starch during gelatinisation: A liquid crystalline approach. *Carbohydrate Research*, *328*, 165–176.
Wrigley, C. W., Booth, R. I., Bason, M. L., & Walker, C. E. (1996). Rapid Visco Analyser: Progress from concept to adoption. *Cereal Foods World*, *41*, 6–11.